Molecular Crystals and Liquid Crystals

Publication details, including instructions for authors and subscription information:
http://www.tandfonline.com/loi/gmcl20

LIQUID CRYSTALS IN TELECOMMUNICATIONS SYSTEMS

W. A. Crossland [a], T. V. Clapp [a], T. D. Wilkinson [a], I. G. Manolis [a], A. G. Georgiou [a] & B. Robertson [a]

[a] University of Cambridge, Department of Engineering, Trumpington St, Cambridge, CB2 1PZ

Version of record first published: 07 Jan 2010

To cite this article: W. A. Crossland, T. V. Clapp, T. D. Wilkinson, I. G. Manolis, A. G. Georgiou & B. Robertson (2004): LIQUID CRYSTALS IN TELECOMMUNICATIONS SYSTEMS, Molecular Crystals and Liquid Crystals, 413:1, 363-383

To link to this article: http://dx.doi.org/10.1080/15421400490438825

Mol. Cryst. Liq. Cryst., Vol. 413, pp. 363/[2499]–383/[2519], 2004

ISSN: 1542-1406 print/1563-5287 online
DOI: 10.1080/15421400490438825

Taylor & Francis
Taylor & Francis Group

LIQUID CRYSTALS IN TELECOMMUNICATIONS SYSTEMS

*W. A. Crossland**, *T. V. Clapp, T. D. Wilkinson, I. G. Manolis, A. G. Georgiou, and B. Robertson*
University of Cambridge, Department of Engineering, Trumpington St, Cambridge CB2 1PZ

The first liquid crystal devices have recently been installed in the fibre optic networks that provide the backbone of the modern telecommunications system. Most optical network devices are concerned with the manipulation of the amplitude and phase of the optical signal. Liquid crystals have the highest figure of merit for field addressed electro-optic response and can have excellent transparency in the optical telecommunications window.

Here we consider the importance of liquid crystals in controlling the phase and the state of polarisation of light in these systems. We also consider arrays of liquid crystal phase modulators, fabricated using LCOS technology, in holographic switches and multifunction devices.

INTRODUCTION

The global link diagram for a broadband optical fibre transmissions system is usually shown in a block functional form. A typical diagram is shown in Figure 1. It extends from source transmitter to end-receiver and may represent a link several 1000's of kilometres long. Several of the "functional blocks" illustrated may themselves be decomposed into elements which have a logical description as functional blocks. These elements may themselves be composed of sub-assemblies and this recursion extends all the way down to the component level. This sort of diagrammatic representation is more than a useful shorthand notation and it is used by the network systems designers to allocate the "link budget". The process of designing the transmission system begins with a service quality assumption (a bit-error-rate and similar performance measures). The transmitter–receiver pair, in direct linkage, is designed to assure more than adequate performance with sufficient margin to account for the summed degradation due to the fibre

*Corresponding author. E-mail: wac@eng.cam.ac.uk

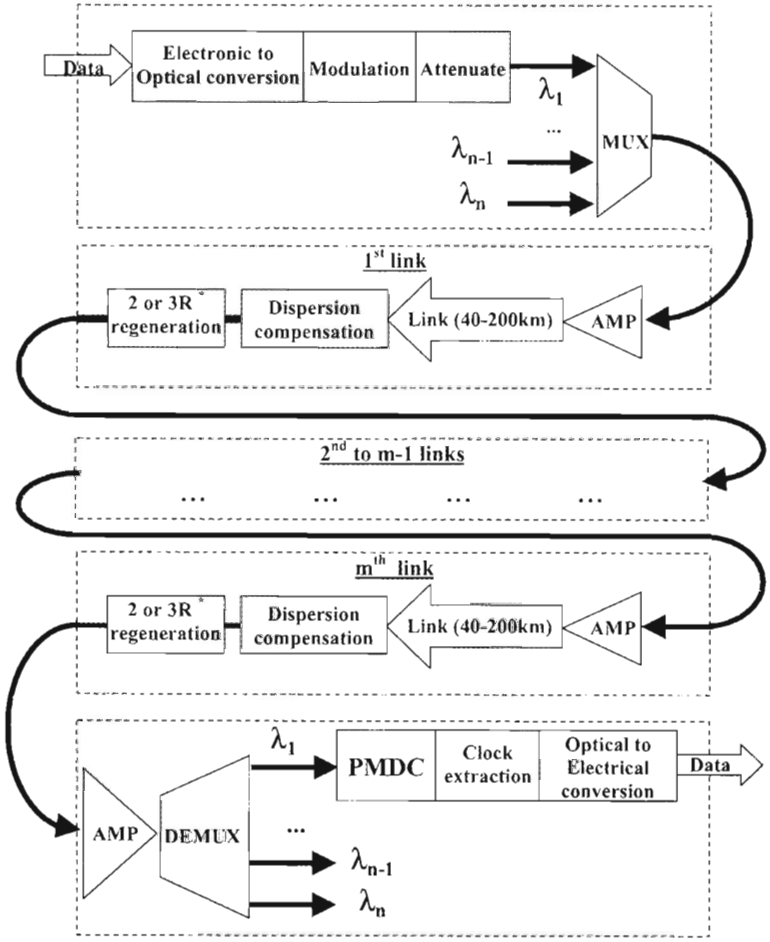

FIGURE 1 Link diagram for an optical fibre transmission system with m links and n wavelength channels. (*) Signal Retiming/Reshaping/Restoration.

transmission plus all the interposed elements. Whenever the signal integrity is degraded to a condition where the receiver (hypothetically placed at that point) could not give the required optical-signal-to-noise ratio then either partial or full signal regeneration is applied.

A very appropriate decomposition of the network would be to depict it as a serial assemblage of units which split, phase adjust, amplify and route the signals. This then reveals an underlying physical fact that mathematically signal transmission can be described as a matrix multiplication of complex

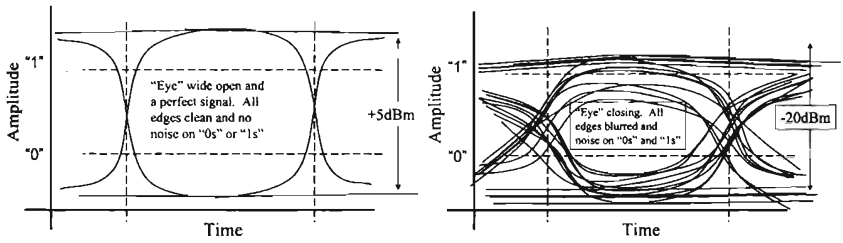

FIGURE 2 Open and closed eye diagrams in a telecommunications system.

transfer matrices which effect changes upon the phase and amplitude of encoded data streams.

Communications engineers would frequently choose to illustrate this via an "eye diagram" which shows the temporal accumulation of data in a "bit-wide" interval of time. The decision circuit of a receiver must operate in an open "eye" where it can (with close to zero error) distinguish between the 0-level and the 1-level of binary encoded data-streams (multi-level encoding complicates this picture only slightly). This is a good way to view the consequences of dispersion, jitter and other signal impairments.

The eye diagram is an ideal way to visualise the state of a signal stream at significant nodes in the transport path. Very close to the transmitter the eye is open and ideally has a perfect rising and trailing edge with every bit sequence in the stream exhibiting identical properties. For most telecommunications links the signalling will require a link budget to be established which sets the launch power and signal impairments which can be tolerated so that the receiver can achieve a low bit-error-rate. For high performance broadband links the error rate may be better than 1 error in every 10^{15}.

By the time the signal has passed over several 10 s of kilometres the combination of signal attenuation and dispersion results in significant eye closure. However, optical amplification can recover the signal and open the eye sufficiently that a receiver's decision circuit would still be able to decode the signal.

The ability to intervene in the optical domain to reverse both the worst effects of attenuation and chromatic dispersion have enabled links to be concatenated to upwards of 2000 km before it is necessary to do a full 3 R (Restore/Re-amplification, Retime, Reshape) regeneration of the signal as shown in Figure 1. In the past this would have set the spacing of the electronic (O-E-O) regenerators but now that such large distances have been enabled for many routes it is not necessary. There is now great promise that full optical regeneration is possible.

If we look more closely at the eye at the receiver we can provide interpretation of the impairments which have occurred. For the rising

and trailing edges some "smearing" in time is evident. Much of this is due to the dispersion of the signal. The different wavelength components of a "bit" are being differentially delayed. This is due to the fact that for most fibre the slope of the effective refractive index dispersion will have meant that the shorter wave portion had "further" to go! The chromatic dispersion correction that is applied is very seldom accurate and so it is inevitable that some smearing occurs. This is also true for the ortho-normal polarisation components of the optical signal. If a fibre were perfectly cylindrical and symmetric then laid out in a straight path it would be totally degenerate with respect to polarisation state of the transmitted signal. i.e. all the light would propagate with a constant phase velocity. However, fibre is never perfect and it is then cabled, spooled, strung through conduit and on poles which breaks the symmetry. So all real installed optical links are a concatenated sequence of pseudo-random wave-plates. It is this that leads to the occurrence of polarisation mode dispersion as depicted in Figure 3. In addition fibre optical non-linearity (whilst small) does cause self phase modulation of the bits (dependent on their instantaneous power) consequently some of the dispersion cannot be corrected by simple chromatic or PM dispersion correction.

By the time the non-linear propagation effects, signalling amplitude decay, cross-talk, noise etc have all been convolved the signal envelope has distortion which it may well prove impractical (possibly impossible) to repair. However, if one had more distributed partial restoration (in the optical domain) then the transport distances could be improved dramatically. For this to be practical very highly functional and low-cost modules would need to be manufactured. The primary mechanism would be accurate phase control combined with polarisation state intervention (ideal for LCs).

Simple wave-plates, like the one shown in Figure 3, for inclusion in optical trains, whether in guided wave or free-space applications, can greatly alleviate problems associated with polarisation dependent loss

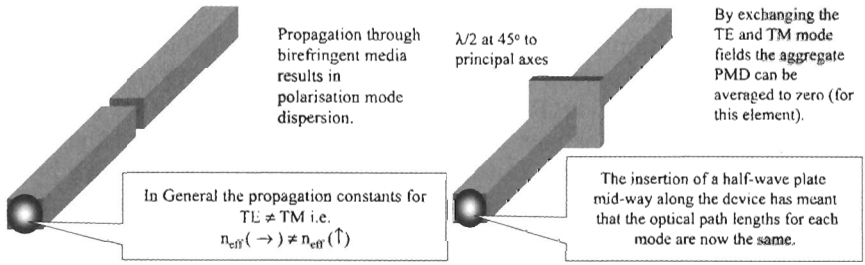

FIGURE 3 Birefringence in waveguide structures.

and polarisation mode dispersion. For the very highest signalling rates the effects of polarisation mode dispersion are very severe. So much so that at 40 Gb/sec it is believed that dynamic PMD correction will be required and that individual links may need to be shorter. In general, the birefringence associated with these links is not predictable and may drift with time. Hence, these principles need to be applied to adaptive phase control devices. Such elements are readily derived from liquid crystal technology.

The cost of carrying out optical to electronic conversion on these high capacity data streams means that optical switching must be carried out at nodes in the network in order to control and manage the traffic ('optical transparent cross-connects'). Currently the leading technology for scalable switches of this kind is MEMS (Microelectromechanical Systems) in which small mirrors are used to deflect light beams between optical waveguides. Efficient beam deflection can also be carried out using arrays of liquid crystal pixels arranged as phase gratings or holograms [1]. This is illustrated in Figure 4. Each pixel is in effect a waveplate. The light power deflected by such holograms can be independent of the polarisation state of the incoming beam and in a perfect beam deflector of this type no photons would be lost. The remarkable optical flexibility of liquid crystal holograms should allow optical channels to be adaptively manipulated and controlled in ways that are not possible with simple mirrors.

LIQUID CRYSTAL DEVICES AS POLARISATION MODULATORS

There are many different electro-optical effects available from liquid crystal devices. For some telecommunications applications these effects must display some form of polarisation insensitivity despite the birefringence of liquid crystals, as the polarisation state in an optical fibre network is often unknown or changing with time. There are several different types of polarisation rotation effects and phase modulation effects, which can be used in

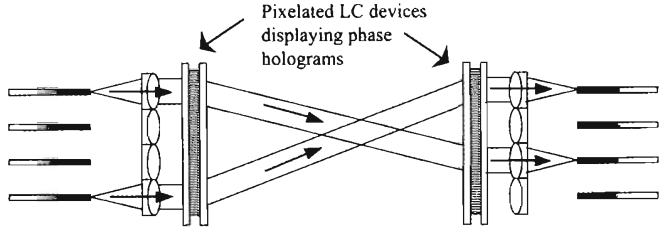

FIGURE 4 Scalable free-space switch architecture using two holograms. Note: The reconfigurable liquid crystal holograms are envisaged as reflective LCOS (liquid crystal over silicon) devices, but are shown here for simplicity as transmissive structures.

these applications. Two of the most useful for telecommunications are binary phase modulation with ferroelectric LCs (FLCs) and multi-level phase modulation with nematics LCs (NLCs). In order to appreciate the role of these effects, it is important to analyse the characteristics of both FLC and NLC modulation.

A surface stabilised FLC (SSFLC) cell is optically equivalent to a rotating retardation plate with an in plane tilt of 2θ, where θ approaches the tilt angle of the smectic cone. We can describe the effect of a retardation plate on an incident plane wavefront of light using Jones analysis. Elliptically polarised light describes any input polarisation of light in a given xyz coordinate system and is given by the formula:

$$IN = \begin{bmatrix} \cos\psi \\ e^{j\delta}\sin\psi \end{bmatrix}$$

were δ is the phase difference between the horizontal and vertical component of polarisation and ψ is the inclination of the polarisation ellipse. Assuming that the retardation plate is placed with its slow axis (mean molecular axis of the SSFLC cell) at a random angle α to the x-axis, its representation in the coordinate system x'y'z' is shown in Figure 5.

Polarisation components travelling along the molecular axis experience the extraordinary refractive index n_e and components travelling normal to it experience the ordinary refractive index n_o. The phase retardation between those two components on exit of the cell will be $\Gamma = k_0 d\Delta n$ radians, where $k_0 = 2\pi/\lambda$ is the wavenumber in the free space, d is the thickness of the cell, and $\Delta n = n_e - n_o$ is the birefringence of the material at the operational wavelength. The corresponding Jones matrix for the cell will be:

$$S = \begin{bmatrix} e^{-jk_0 d\Delta n}\cos^2\alpha + \sin^2\alpha & \sin\alpha\cos\alpha\left[e^{-jk_0 d\Delta n} - 1\right] \\ \sin\alpha\cos\alpha\left[e^{-jk_0 d\Delta n} - 1\right] & e^{-jk_0 d\Delta n}\sin^2\alpha + \cos^2\alpha \end{bmatrix}$$

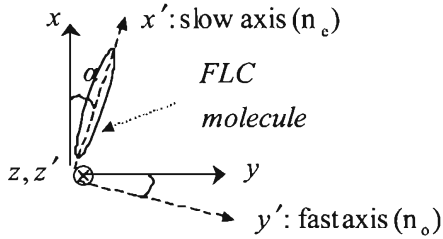

FIGURE 5 Coordinates of a molecule in an SSLLC cell.

Then, the polarisation state of the output light (after the retardation plate) is calculated through the relation:

$$OUT = S \cdot IN$$

When the thickness of the LC layer is such that the overall retardation between fast and slow components is equal to π (half-wave plate configuration), then the cell acts as a perfect polarisation rotator around the optical axis defined by the direction of the molecules. In general however, $\Gamma \neq \pi$, and the output light is polarised into an elliptical state, which is non-symmetrical to the input state with respect to the optical axis. We can take advantage of the polarisation rotation properties of an SSFLC cell and con figure it as a binary, phase-only modulator as shown in Figure 6. The FLC cell is placed between crossed polarisers so that the input polarisation bisects the two switching states of the liquid crystal. For the two switching states in Figure 6, it is $\alpha = \theta$ and $\alpha = -\theta$ respectively. Hence, we obtain two output states:

$$OUT(1) = +\sin(|2\theta|) \cdot \sin(k_0 d\Delta n/2) \cdot \exp(-j \cdot const)\hat{y}$$
$$OUT(2) = -\sin(|2\theta|) \cdot \sin(k_0 d\Delta n/2) \cdot \exp(-j \cdot const)\hat{y}$$

It can be seen that the two components have the same polarisation state (linear along y-axis) and the same amplitude, however they display a relative phase difference of π radians. The π-phase modulation is independent of the cell parameters Γ and θ. In this arrangement, there is an associated energy loss, which is caused by the introduction of the analyser in the optical path of the beam. The overall optical transmission is:

$$T = \sin^2(2\theta)\sin^2(k_0 d\Delta n/2)$$

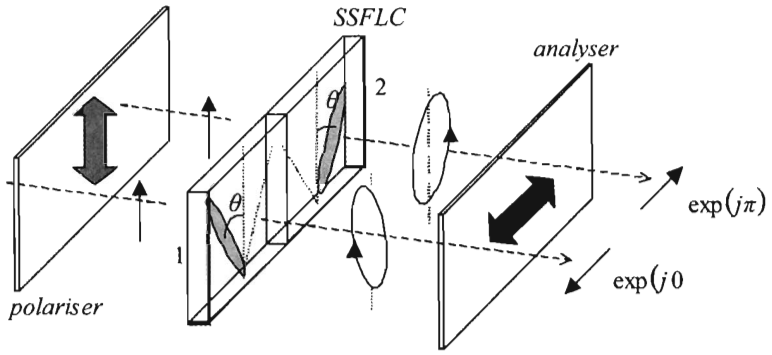

FIGURE 6 The two switch states in a SSFLC cell.

The configuration of an FLC spatial light modulator for the implementation of a free-space diffraction-based optical crossbar in an arrangement like the one shown in Figure 6 (i.e. using crossed polars) was initially proposed by O'Brien *et al.* [2]. Experimental demonstration, however, of a programmable binary phase-only SLM based on FLCs, capable to record in real time computer generated holograms (CGHs), and evaluation of its performance was first reported by Broomfield *et al.* [3].

It can be shown however, that the phase modulation capabilities of FLC devices are in fact preserved even when the polarisors are removed out of the path of the beam. More specifically, the performance of an FLC SLM configured to display a binary phase hologram is independent of the input polarisation state and it is only limited by the cell parameters, the optimal values being an optical thickness of π radians and an aggregate switching angle of 90 degrees. The principle for polarisation-insensitive operation of FLC devices was first analysed and demonstrated for switchable fixed-grating reflectors by O'Callaghan *et al.* [4] and described more rigorously later by Warr *et al.* [5] in the context of reconfigurable holographic switches. We can easily demonstrate the validity of this concept by considering the input light to be decomposed into two orthogonal polarisation components, which are diffracted by the hologram in an identical way. For both components, the pattern obtained at the replay field as well as the corresponding diffraction efficiency is exactly the same, and therefore the total intensity distribution from the two overlapping patterns remains the same independently of the polarisation state of the input light.

There are an infinite number of ways to decompose the light of unknown polarisation into two orthogonal, linearly polarised components. Here we choose to decompose the input light along the two bisectors of the angle formed by the two switching states of the molecular director (state-1 and state-2) in Figure 6. This particular choice greatly simplifies the analysis. In Figure 7(a) and (c), the two components of the input light are shown separately, along with the two switching states of the liquid crystal and the chosen system of coordinate axes. The two components are along the x- and y- axis correspondingly and they are noted in the figure using the symbols IN_X and IN_Y.

We have already calculated the matrix S that describes the effect of the LC film on the input plane of light in the xyz coordinate system of axes. In the first case, we consider only components of the input light polarised along the x-axis (i.e. IN_X components). Performing the calculation, we find for the polarisation state of the light at the output plane:

$$OUT = \begin{bmatrix} OUT_x \\ OUT_Y \end{bmatrix} = \begin{bmatrix} \exp[-j(k_0 d\Delta n/2)]\cos^2 a + \sin^2 a \\ \sin(2\alpha)\sin(k_0 d\Delta n/2)\exp[-j(k_0 d\Delta n/2 + \pi/2)] \end{bmatrix}.$$

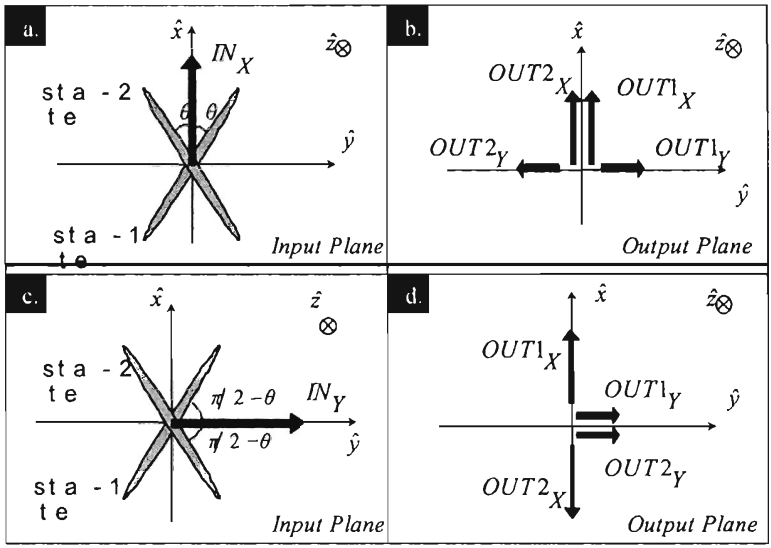

FIGURE 7 Orthogonal components in the binary phase states of an SSFLC.

We note that α is the angle between the optical axis of the cell (molecular director) and the x-axis of the coordinate system. OUT_X and OUT_Y represent the polarisation components of the output light along the x- and y-axis respectively. As expected, since the analyser is not in place anymore, the expression for the output field contains also a non-zero component along the direction of the x-axis. The output polarisation components, which corresponding to the two switching states of the LC cell (state-1 and the state-2), are calculated using $\alpha = \theta$ and $\alpha = -\theta$ in the above equation. It is very important to observe at this point that whereas the expression for the OUT_Y component is an odd function of the angle α, the corresponding expression for the OUT_X component is an even function instead. Subsequently, the x-components of the light exiting the two opposite switched pixels (see Fig. 6) will be equal and *in phase* at the output plane, however, the y-components will be equal but *out of phase* by a factor of π radians. These polarisation components are shown in Figure 7b. The numbers 1 and 2 are used to show, which switching states these components correspond to. Arrows pointing at the same direction or at opposite directions indicate that the corresponding fields are *in-phase* or *out-of-phase* respectively.

In practical terms, if we start with all the energy of the input light polarised along the x-axis, i.e. polarised along one of the two bisectors of the FLC switching angle, only a portion of this light will in effect 'feel'

the presence of the hologram on its way through the LC film and as a result will be diffracted to the corresponding diffraction orders. More specifically, the portion of the light, which, on exit from the film, is polarised along the y-axis, i.e. perpendicular to the initial polarisation direction, will be wholly phase-modulated (with a phase shift of π radians between state-1 and state-2). The rest of the light, i.e. the x-components of the light at the output plane, will remain unmodulated and therefore will be directed straight to the zeroth order of the hologram. The diffraction efficiency of the hologram in this case will exclusively determined by the energy carried by the y-components of the output light. Hence the efficiency will be:

$$n_x = \sin^2(2\theta)\sin^2(k_0 d\Delta n/2)$$

In the above equation, which, of course, is identical to the one given earlier, the symbol n_x is used to note that this is the hologram efficiency when all the input light is polarised along the x-direction.

For the second case, the input light is wholly polarised along the y-direction (this is the second bisector of the ferroelectric switching angle – see Fig. 7c). This case is highly symmetrical to the previous one and we can readily determine that, in this occasion, whereas the y-polarisation components of the light at the output plane, (i.e. those parallel to the initial polarisation direction), are equal and *in-phase*, the x-components are equal but *out-of-phase* by π radians as in Figure 7d. Similarly, the diffraction efficiency of the hologram in this case will be given by the last formula substituting θ with $\pi/2 - \theta$:

$$n_y = \sin^2(2(\pi/2 - \theta))\sin^2(k_0 d\Delta n/2) = \sin^2(2\theta)\sin^2(k_0 d\Delta n/2)$$

We conclude from the above equation that $n_x = n_y$, and hence the overall diffraction efficiency of the hologram will be also given by the same expression, even in the most general case of randomly polarised input, i.e. independently of the energy distribution between its two orthogonal polarisation components and their corresponding phase relationship. Finally, since the hologram pattern is determined by the distribution of the switched states on the LC plane (hence not a property of the input light), this is common for both input polarisation components, and therefore the two diffraction patterns will be also identical and overlap perfectly. This ensures that the power of each diffraction order will remain the same for all possible input polarisation states, and hence the hologram is said to operate in a polarisation insensitive way.

POLARISATION INSENSITIVE PHASE MODULATION USING NEMATIC LIQUID CRYSTALS

Polarisation insensitive holograms, useful in optical switches, can be also recorded using NLCs. The underlying principle has been reported in the literature already; in the first case for the implementation of an intra-chip interconnection pattern useful in clock distribution among electronic chips [6] and in the second case for wavefront correction useful in astronomical applications for image sharpening [7]. Shutters for unpolarised light [8] and a variable, polarisation-insensitive LC phase retarder [9] have been also demonstrated using the same concept. Here we use the principle to generate reconfigurable pixellated multilevel phase holograms to steer the near infrared light from single mode optical fibres such that the power in the routed beam is independent of the state of polarisation of the incoming light.

A pixelated planar nematic device is combined with a quarter wave-plate (QWP) and a mirror (M) in a reflective configuration as shown in Figure 8. The QWP is aligned with its fast axis on the xy plane and at an angle of 45 degrees away from the optical axis of the NLC layer. In the diagram, the

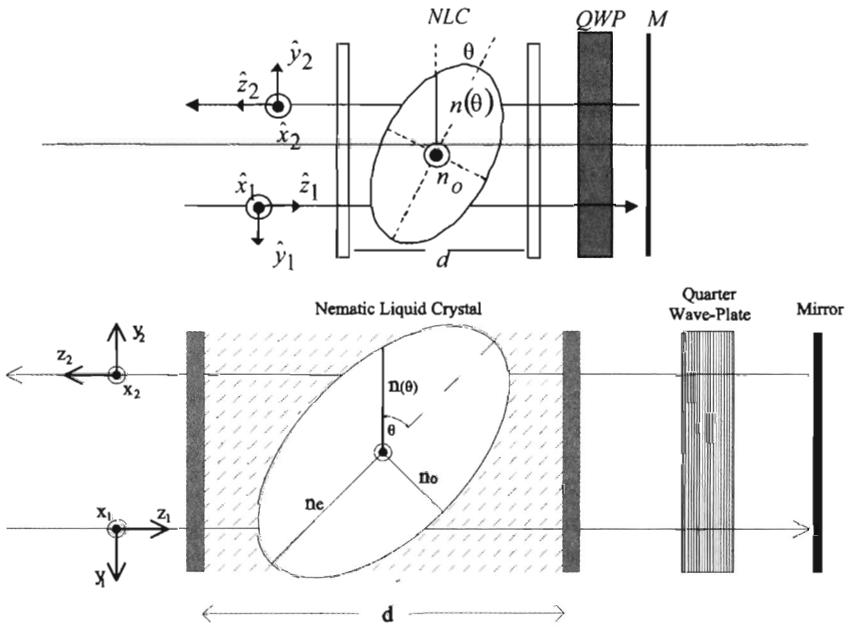

FIGURE 8 Arrangement for polarisation insensitive nematic phase modulation.

optical axis of the LC coincides with the long axis of the index ellipsoid shown. On the application of a driving voltage, this tilts out of the plane of the cell, at an angle θ.

On the first pass through the device, polarisation components along the y-axis experience the extraordinary refractive index n_e of the nematic material, while components parallel to the x-axis only the ordinary refractive index n_o. The combination of the QWP and the mirror acts as a 90° polarisation-rotator for the two orthogonal components ($-x$ and $-y$) thus mutually exchanging their polarisation states. On the second pass from the device, components, which where previously polarised along the x-axis, are now parallel to the y-axis and therefore experience a refractive index of n_e whereas components previously polarised along the y-axis, are now parallel to the x-axis and they only experience the ordinary refractive index of the material. In that way, during the double pass through the nematic layer, both orthogonal polarisations are subjected to the same overall retardation.

According to Jones matrices, the polarisation of the output beam will be given by the equation:

$$\mathbf{E}_{\mathrm{OUT}} = T \cdot \mathbf{E}_{\mathrm{IN}}$$

In the above, T is the overall modulation matrix, which can be calculated by considering the two passes through the system separately and expressing its various components (LC film, QWP and mirror) in the corresponding coordinate systems. In our analysis we don't include transmission coefficients through glass, ITO and alignment layers. These surfaces modulate the amplitude and the phase of the propagating light in an isotropic way, i.e. independently of the plane of polarisation. Their contribution to the tensor T simply takes the form of a scalar coefficient and therefore they are insignificant to the present analysis. Accordingly, the tensor T is of the form:

$$T = N_2 Q_2 M Q_1 N_1$$

N_1, N_2, Q_1, and Q_2 are the matrices representing the effect of the LC layer and the QWP for the first and second pass (coordinate systems $x_1y_1z_1$ and $x_2y_2z_2$) respectively. The QWP, is oriented with its fast axis at an angle 45° with respect to the y-axis. The matrix T, provides us with the required 'exchanging' functionality. Incorporating the matrices for each individual component, we calculate the overall matrix T:

$$T = \begin{bmatrix} T_{11} & T_{12} \\ T_{21} & T_{22} \end{bmatrix}$$

where

$$T_{11} = 0,$$
$$T_{12} = [-d(a_o + a(\theta))] \cdot \exp[-j(dk_0(n_o + n(\theta)))],$$
$$T_{21} = \exp[-d(a_o + a(\theta))] \cdot \exp[-j(dk_0(n_o + n(\theta)))] \cdot \exp(j\pi), \text{ and}$$
$$T_{22} = 0.$$

and k_0 is the wavenumber, d is the thickness of the NLC, a represents the absorptive properties of the NLC and n represents the refractive index of the NLC. Finally, we get for the state of the output light:

$$\mathbf{E}_{\text{OUT}} = \begin{bmatrix} \rho_y \cdot \exp[-d(a_o + a(\theta))] \cdot \exp[-j(dk_0(n_o + n(\theta)) - r + \pi)] \\ \rho_x \cdot \exp[-d(a_o + a(\theta))] \cdot \exp[-j(dk_0(n_o + n(\theta)))] \end{bmatrix}$$

We conclude from the last equation that, for any tilt angle the two orthogonal polarisation components receive the same amount of phase retardation and amplitude attenuation. As a result, a spatial arrangement of switching states across the xy-plane, by means of a pixellated device (SLM) for example, produces exactly the same holographic pattern for both polarisation components. Consequently, the two components diffract in a similar way thus resulting into two identical and perfectly overlapping diffraction patterns. The intensity distribution of the two patterns on the replay field is exactly the same for the two components and therefore the total intensity of each diffraction spot is ultimately preserved independently of the amplitude/phase ration between the two input components, thus independently of the input polarisation state. This is equivalent with obtaining polarisation insensitivity in the operation of a holographic switch, where the diffraction spots of the hologram are used to launch the light into the output fibres of the switch.

In order to validate the potential of the arrangement, in particular with relation to its application in optical fibre-switches, a series of experiments and simulations have been carried out aimed to demonstrate the polarisation insensitivity of the proposed double-pass architecture and its capability to multi-level phase operation [10].

PHASE HOLOGRAMS IN TELECOMMUNICATIONS SYSTEMS

In this section we describe aspects of the design of multiphase spatially quantised holograms for use in optical networks. These reconfigurable holograms are written to arrays of liquid crystal pixels. Each pixel is a phase modulator. The modulators are envisaged as being capable of 2 π phase excursion and large arrays of such reflective pixels can be produced

over silicon VLSI circuits using LCOS [1]. The pixel size might be of the order of 10 microns.

A single reconfigurable holographic beam steering element might be used in a 1: N port switch [1] (capable of multicasting and extracting monitoring channels). In general the polarisation state of the incoming light is unknown, so the beam deflector should be polarisation insensitive. Binary phase modulators using ferroelectric modulators are in many ways ideally suited to this task, but due to the symmetry of the hologram, light is deflected into both positive and negative first order beams. This usually means that half the light is lost. This may not be acceptable, especially in $N \times N$ port switches (such as shown in Figure 4) where two beam deflecting holograms are required. This loss can be avoided by using polarisation insensitive multilevel phase modulators as described above. The hologram is then analogous to a blazed grating and can in principle direct the entire incident light into the deflected beam with no loss of photons.

Beam deflection can be very precise (see below) and only depends on the pattern presented, so is both robust and reproducible.
The method described is able of:

- Create any number of bright spots on the replay field where the output fibres are positioned, making possible holographic beam steering switch structures such as shown in Figure 4.
- Equalise the signal amplitude arriving from the input ports.
- Control the phase of the output ports.
- Reduce noise at particular points or areas on the replay field where non-output fibres are placed thus reducing crosstalk.
- Fine-tune the hologram in order to compensate mechanical inaccuracies.

The replay field in a 4f arrangement of a pattern of pixels, or hologram, is given by the Fourier transform of that pattern [11]. For the telecommunications network components the problem is usually to design a phase hologram in order to create a single spot on the replay field with a given phase. In this case it is possible to reduce the problem from global to a localised one by considering the useful contribution of each pixel to the output port. The resulting hologram will be a blazed grating as shown in Figure 9.

However, a continuous phase blazed grating can not be displayed in a LC device without being quantised in terms of space and phase. The phase value of the pixel in this case is chosen so the phase difference is minimised. Figure 10 shows the result when a continuous phase blazed grating is quantised to four phase levels. Also it shows the replay field of the hologram, which now contains a different noise floor due to the quantisation process. This is a major problem in telecommunications applications as it

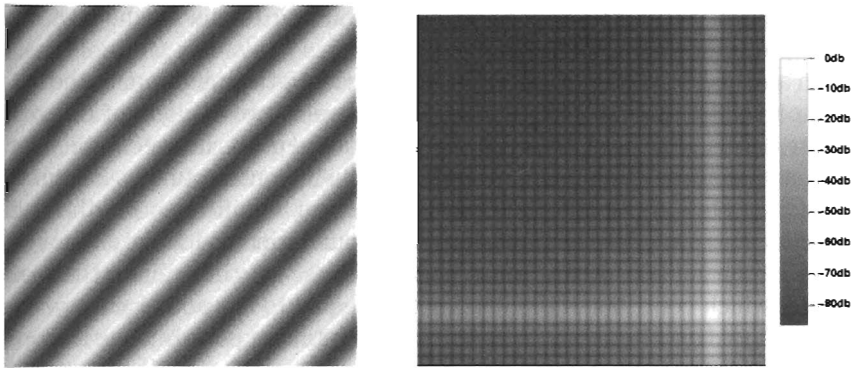

FIGURE 9 Hologram and replay field of a typical blazed grating (the desired port position is in the lower right hand corner). The replay field was evaluated taking into account the finite hologram size.

creates unwanted crosstalk. This noise is structured and has created a peak in the upper left corner, giving a crosstalk at this point of −20dB.

The hologram in Figure 10 is not optimal in terms of crosstalk, hence it must be redesigned to reduce the structure in the noise floor. This is achieved by cancelling out noise and creating a dark point on the replay field where a non-output fibre is placed. This is a similar process to creating a bright spot but in this case there is already some E-field at the point of interest. Therefore it is desirable to create another spot of equal intensity on top of it but with opposite phase in order to cancel each other resulting into minimum intensity. At the same time the diffraction efficiency of the hologram has to be affected minimally. This is achieved by adapting

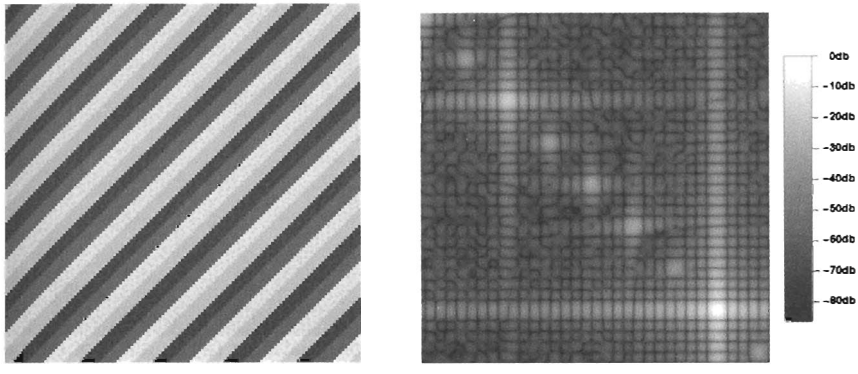

FIGURE 10 Four phase level quantised blaze grating and associated replay field.

the value of the pixels that contribute minimum to the bright spot and contribute maximum to the dark point.

In any blazed grating the pixels that contribute the minimum to the output port are the ones on the boundary between two regions of different phase levels. In these boundaries the disagreement between the ideal and actual phase is maximum and thus their contribution is minimum (see Fig. 11a). Similarly, pixels with maximum significance for the dark spot are the ones further away from the boundaries which lie on straight lines in the middle of the same phase stripes. On these lines the ideal phase, which contributes the maximum, is equal to the actual phase value (as in Fig. 11b). Therefore, in order to have optimum performance it is preferred to change the pixels that lie on the intersections of lines that contribute minimum to the output port and maximum to the dark point (Fig. 11c). Note that in this figure the pixels affected are marked in a circle. Their actual shape will depend on the importance of crosstalk over efficiency. An efficiency demanding design will create ellipsoids expanded diagonally, along the pixels' boundaries of Figure 10a. Alternatively, if crosstalk is more important then the ellipsoids will expand horizontally.

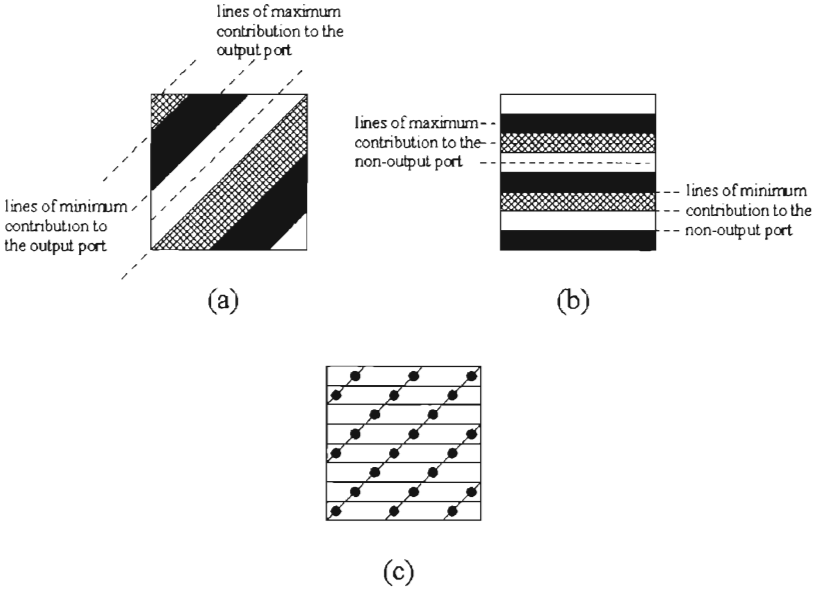

FIGURE 11 The three-phase grating required for creating a (a) single spot on the replay field, (b) a single spot where noise is to be reduced. (c) The optimum pixels to be altered.

It might be the case that these ellipsoids are so long and thin that will merge forming a single line, diagonally or horizontally.

This design concept was verified by designing a hologram using simulated annealing where the noise at a particular *point* was required to be minimised. The resulting hologram followed most of the above predictions. The pixels that were modified belonged on the lines which their contribution to the non-output port was maximum. Even though the non-output port was placed on top of a secondary order, the crosstalk was reduced from an initial value of -26 dB down to -60 dB with only 0.1 db decrease on the output power.

Sometimes if is desirable to reduce the noise from a certain *area* instead from particular point especially if fibres with large diameter are used. This is achieved by forming an array of dark points. The quantised four-phase hologram was modified using simulated annealing to form the hologram shown in Figure 12 where a square of low noise on the replay field was formed. The noise within this area was reduced by 25 db even if the square was placed on top of a secondary order.

FINE TUNING OF HOLOGRAMS

While holograms are spatially quantised in terms of their pixels the replay field is not. Instead, it is possible to route light to practically any point in the replay field with extreme accuracy by adjusting the pattern on the hologram. This reduces the need of high tolerances on the positioning of fibres which is vital when single mode fibres are being used. Also, it can be used

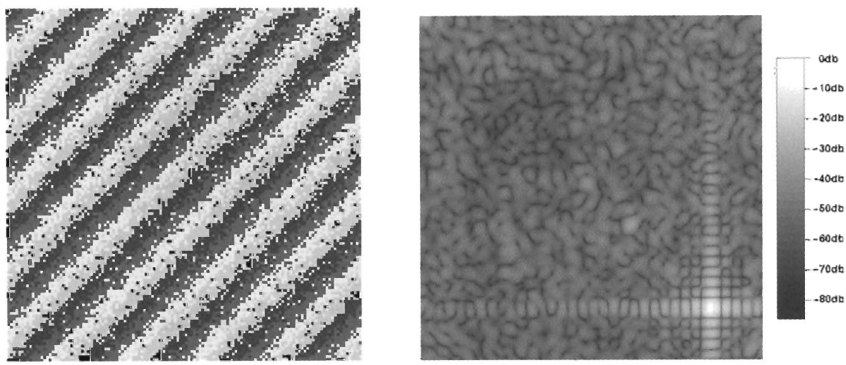

FIGURE 12 Four level blazed grating created by simulated annealing and its associated replay field. The noise peaks has been actively suppressed in the algorithm.

to compensate for mechanical vibrations and positional errors in the manufacturing, thus reducing the production costs.

In a practical demonstration of this the deflection angle was varied by changing the pattern on a 540 × 1 FLC hologram while keeping the position of the fibre fixed [12]. It was possible to fine-tune the hologram with accuracy of a fraction of a μm and thus achieving maximum coupling into the fibre. The spot on the replay field had a Gaussian profile (due to the Gaussian illumination profile on the hologram) and by scanning it across the fibre the coupling power was also varied. By knowing the theoretical position of the spot and the numerical aperture of the fibre it is possible to predict the in-coupled power. Doing so it was found that the experiment followed with great accuracy the expected in-coupled power demonstrating sub-micron accuracy movement on the spot (Fig. 13).

The parameters of the above design, like focal distance of the lens and wavelength, were known so it was possible to define positions on the replay field in μm. When these parameters are unknown is essential to use a normalised length unit that is affected only by the hologram pattern. In general, the maximum achievable deflection from a pixelated hologram occurs when its pixels form a chequerboard pattern. This is the highest spatial frequency which can be achieved for any hologram. Consequently, we define the useful replay field (URF) length as the side of the square

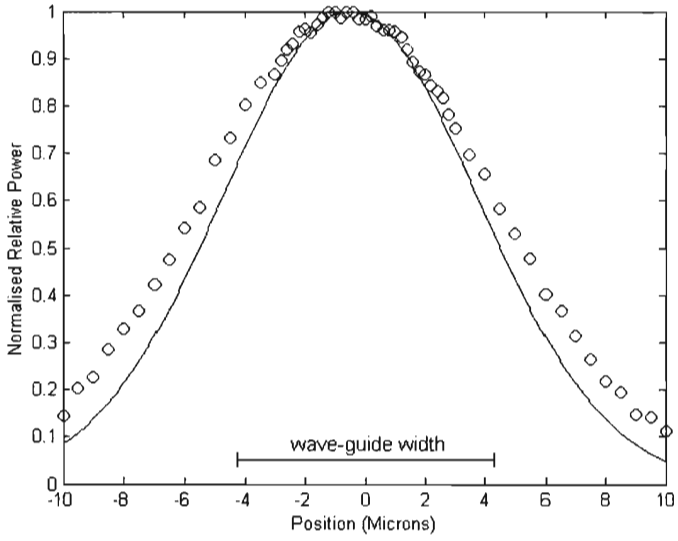

FIGURE 13 Measurement of the in-coupled power into the fibre when the spot was scanned across the waveguide.

formed by a first order spot of the chequerboard hologram and the zero order (see Fig. 14).

A test to determine the accuracy in which a hologram can position a spot in the replay field was run. A hologram was designed by attempting to achieve maximum intensity at a particular point in the replay field. Then a search algorithm was used to determine the actual spot position. Comparing the actual and the desired position of the spot the positioning error (in URF units) was calculated.

It is expected that the error in position is dependent on where the spot is on the replay field. This dependence is encouraged by the pixelated nature of the hologram, which favours spatial periods of integer number of pixels. This was proved by scanning the position of the routing beam in a linear fashion from (0.0, 0.2) to (0.25, 0.2) in 500 steps. For each step a hologram was designed and the positioning error was evaluated. The hologram had intentionally only 64×64 pixels in order to increase accuracy errors and reduce running times. The scanning was repeated multiple times and produced similar plots. One of these plots is shown in Figure 15 where the error is plot as a function of the spatial co-ordinate u of the replay field.

It was observed that the error on average was very small (4×10^{-6} URF units) but had peaks of large error which followed a regular pattern. Errors smaller than five times the average error were less repeatable showing that they were due to statistical aberrations of the simulated annealing. On the other hand, larger errors were repeatable demonstrating an incapability of the hologram to route light effectively to these positions. Also, for small deflections of the beam (< 0.02 URF units) the error on the position was considerably larger. Large errors occur at regular intervals because on

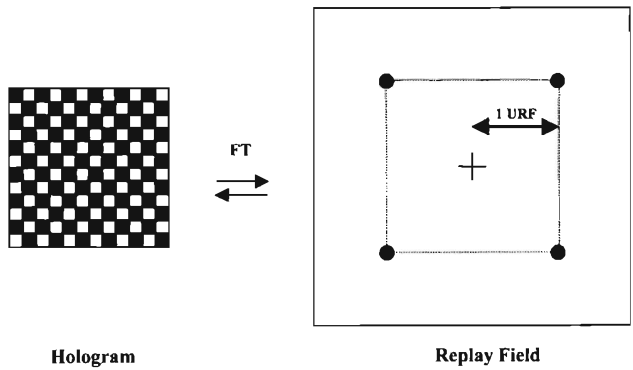

FIGURE 14 The unit URF is defined as the maximum horizontal or vertical distance of a first order from the zero order. The shaded area of the replay field shows the positions where fibres can be placed.

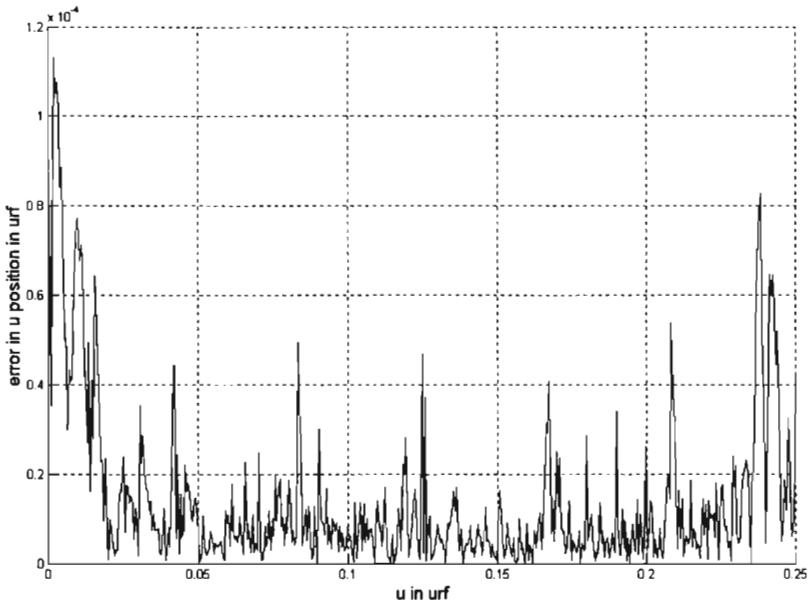

FIGURE 15 A plot showing the error in positioning spots in the URF.

these positions the period size is an unfavourable non-integer number of pixels. Also, near the zero order position, errors are larger because the hologram is small relative to the spatial period required. This makes it unattractive to use the area near the zero order because it will not enable adaptive fine tuning.

We have argued that the optical functions that can be carried out by liquid crystal devices are remarkably well matched to many of the challenges facing telecoms and datacoms networks e.g. phase control is a major issue and no other materials match liquid crystals for the magnitude of their electro-optic response or their transparency. The same basic flexibility in the materials may extend to their properties that are related to wavelength dispersion and optical non-linearity.

Arrays of phase modulators, integrated with silicon VLSI using LCOS technology appear to allow further levels of flexibility in that beam steering, wavefront correction, control of crosstalk and phase, and channel equalisation etc. appear possible in integrated device structures.

Adapting liquid crystal materials and their electro-optic structures to these challenges has just commenced. This will hopefully go on alongside the exploration of new device structures and the consideration of the many packaging and reliability issues that need to be addressed.

REFERENCES

[1] Crossland, W. A., Manolis, I. G., Redmond, M. M., Tan, K. L., Wilkinson, T. D., Holmes, M. J., Parker, T. R., Chu, H. H., Croucher, J., Handerek, V. A., Warr, S. T., Robertson, B., Bonas, I. G., Franklin, R., Stace, C., White, H. J., Woolley, R. A., & Henshall, G. (Dec. 2000). Holographic optical switching: the 'ROSES' demonstrator, *J. Lightwave Technol.*, *18*, 1845–1854.

[2] O'Brien, D. C., Crossland, W. A., & Mears, R. J. (1991). A holographically routed optical crossbar: theory and simulation. *Optical Computing and Processing*, *1*(3), 233–243.

[3] Broomfield, S. E., Neil, M. A. A., Paige, E. G. S., & Yang, G. G. (1992). Programmable binary phase-only optical device based on ferroelectric liquid crystal SLM. *Electronic Letters*, *28*(1), 26–28.

[4] O'Callaghan, M. J. & Handschy, M. A. (1991). Diffractive ferroelectric liquid-crystal shutters for unpolarised light. *Opt. Lett.*, *16*(10), 770–772.

[5] Warr, S. T. & Mears, R. J. (April 1995). Polarisation insensitive operation of ferroelectric liquid crystal devices. *Electronics Letters*, *31*(9), 714–716.

[6] Marom, E. & Konforti, N. (July 1987). Dynamic optical interconnections. *Optics Letters*, *12*(7), 539–541.

[7] Love, G. D. (1993). Liquid-crystal phase modulator for unpolarised light. *Applied Optics*, *32*(13), 2222–2223.

[8] Ulrich, D., Tombling, C., Slack, J., Bonnett, P., Henley, B., Robinson, M., & Anderson, D. (2000). A diffraction based polarisation independent lightvalve, presented at the IEE Seminar on Microdisplay and Smart Pixel Technologies, IEE., pp.8/1–6. London, UK, 17 March 2000.

[9] Morita, Y., Stockley, J. E., Johnson, K. M., Hanelt, E., & Sandmeyer, F. (1999). Active liquid crystal devices incorporating liquid crystal thin film waveplates. *Jpn. J. Appl. Phys.*, Part 1, *38*(1A), 95–100.

[10] Manolis, I. G., Wilkinson, T. D., Redmond, M. M., Crossland, W. A. (2002). Reconfigurable multilevel phase holograms for optical switches. *IEEE Phot. Tech. Lett*, *14*(6), 801–803.

[11] Goodman, J. W. *Introduction to Fourier optics*, Graw-Hill Publishing Company.

[12] Johansson, M., Hard, S., Robertson, B., Manolis, I. G., Wilkinson, T. D. & Crossland, W. A. (April 2002). Adaptive beam steering implemented in an FLC-SLM free-space optical switch. *Accepted in Applied Optics*.